PROCESS INTEGRATION AND EXERGY-BASED ASSESSMENT OF HIGH-TEMPERATURE SOLID-OXIDE ELECTROLYSIS CONFIGURATIONS

Robert Müller[1,*], George Tsatsaronis[1]

[1]Technische Universität Berlin, Chair of Energy Engineering and Climate Protection, Berlin, Germany

*Corresponding Author: robert.mueller.2@tu-berlin.de

ABSTRACT

Solid oxide electrolysis is considered an efficient option for largely emission-free hydrogen production and, thus, for supporting the decarbonization of energy systems, especially the process industry. The thermodynamic advantages of high-temperature operation can be utilized particularly by heat integration from subsequent chemical processes. As the produced hydrogen is usually required for the latter at a higher pressure level, the operating pressure of the electrolysis is a relevant design parameter.

The study investigates pressurized and near-atmospheric designs of solid oxide electrolysis, the integration of process heat from ammonia synthesis, and the inefficiencies that occur in the processes. For this purpose, pinch analysis is used to estimate the potential of heat integration. Subsequently, exergy analysis is applied to compare the different design options in terms of efficiency and to identify optimization potential. It can be shown that pressurized operation does not necessarily lead to advantages in efficiency if no sweep gas utilization is applied. In this context, the air ratio is considered as a particularly relevant influencing factor.

1 INTRODUCTION

Hydrogen produced in a largely CO_2-neutral manner is widely regarded as an essential component of future energy and material systems. One possible technical approach is the production of so-called "green" hydrogen using water electrolysis which is powered by electricity generated from renewable energies. Solid oxide electrolysis (SOEL), which usually operates at a high-temperature range between 700–900 °C (Min et al., 2022), shows efficiency advantages compared to other electrolysis technologies since the evaporation enthalpy as well as part of the total energy required for water splitting can be provided thermally and the process further benefits from improved kinetics and lower internal resistances (Buttler and Spliethoff, 2018). This has particular advantages if heat from other processes can be incorporated, e.g., by integration of process heat from exothermic downstream processes like methanation, ammonia, methanol or Fischer-Tropsch synthesis which require a hydrogen supply (Hauch et al., 2020).

Most of the downstream synthesis processes in question are currently operated at elevated pressures. These range, e.g., from 20–40 bar for Fischer-Tropsch synthesis (Deutschmann et al., 2011) and 50–100 bar for methanol synthesis (Ott et al., 2012) to 80–400 bar (mainly 150–250 bar) for ammonia synthesis (Appl, 2011). This makes it necessary to supply the hydrogen at a correspondingly high pressure level. Some authors therefore suggest operating the upstream electrolysis at higher pressures, as the compression of liquid water requires significantly less power than the subsequent compression of the gaseous hydrogen produced (Hansen et al., 2011; Posdziech et al., 2019).

As ammonia is considered the second largest chemical synthesis product (Appl, 2011), whose production accounts for approx. 1.8 % of global energy supply and CO_2 emissions (The Royal Society, 2020), its

https://doi.org/10.52202/077185-0043

greenhouse gas-neutral production offers significant leverage for decarbonizing the industrial sector. Furthermore, the so-called "green" ammonia is discussed as a potential carbon-free energy source (Rouwenhorst et al., 2020). The fact that the stoichiometric conversion of hydrogen and nitrogen to ammonia is associated with a heat of reaction of approx. $46\,\mathrm{kJ/mol_{NH_3}}$ offers interesting opportunities for heat integration with upstream hydrogen production processes. At the same time, the above-mentioned question regarding the efficient provision of the required hydrogen pressure arises.

Pressurized SOEL operation was investigated theoretically (Henke et al., 2011) and experimentally (Jensen et al., 2010; Jensen et al., 2016; Riedel et al., 2019; Riedel et al., 2020) up to 25 bar: While the open-circuit voltage slightly increases due to thermodynamic reasons, the internal resistances decrease and the reaction kinetics are enhanced at higher pressures which can lead to lower area-specific resistances and therefore a lower required active area. A commercial prototype coupled with a methanation plant has already been tested at a pressure of 15 bar (Posdziech et al., 2019).

The aforementioned investigations were mainly carried out at cell or stack level or in the small-scale prototype range. In addition, further simulation-based work has been carried out to investigate the coupling of SOEL at elevated pressures with downstream methanation (Wang et al., 2019) and Fischer-Tropsch (Samavati et al., 2018) processes on a system level.

On this basis, the present study investigates the effect of the pressure level on the efficiency of the SOEL with simultaneous heat integration from a downstream ammonia synthesis applying the Haber-Bosch process. The potential for internal heat recovery is first estimated using pinch analysis. Furthermore, the minimum heating requirement to be supplied externally is determined. Subsequently, exergy analysis is applied to determine the process-internal irreversibilities and to compare the process concepts on the basis of their true thermodynamic efficiencies.

2 PROCESS MODELING

For the intended comparison, two SOEL designs, one pressurized and a second one operated near atmospheric pressure, are each modeled in Aspen Plus®. As a subsequent process, which is not explicitly modeled here, an indirectly cooled ammonia synthesis reactor is selected which was presented by Luyben, 2012, analyzed by Penkuhn and Tsatsaronis, 2017 applying advanced exergy analysis and further adapted and analyzed by Penkuhn, 2023. The process parameters used here refer to the latter but the hydrogen mass flow is scaled down to $\dot{m}_{\mathrm{H_2}} = 1\,\mathrm{kg/s}$ (and thus also the available heat of reaction of the ammonia synthesis) since this results in a more realistic size of the SOEL.

The hydrogen is required at a pressure of approx. 23 bar (Penkuhn, 2023). Taking pressure losses into account, the SOEL stack in the pressurized design A should therefore be operated at 25 bar. In the near-atmospheric design B, the stack is operated at a slight overpressure of 1.5 bar and the hydrogen produced is compressed subsequently. Furthermore, both designs are examined for the case with and without integration of the heat of reaction from the ammonia synthesis. This results in four different variants, which are described in more detail below.

2.1 System description

The four SOEL designs (A1/B1/A2/B2) are shown collectively in Figure 1. In the basic variants A1 and B1, the pressurized and the near-atmospheric design are considered as stand-alone variants without integrating the heat of reaction of the ammonia synthesis. The entire thermal energy must be provided electrically and by internal heat recovery. The subsequent designs A2 and B2, on the other hand, take into account the integration of the heat of reaction from the ammonia synthesis. All heat exchangers are initially considered here as simple heat sources or heat sinks (modeled as HEATER blocks in Aspen Plus). The combination of hot and cold streams to form a heat exchanger network will take place at a later stage.

In all cases, the inlet water is first compressed in pump P1 and then mixed with recycled water in mixer M1. This is followed by preheating (E1), evaporation (E2) and superheating (E3) of the water to stack temperature. In mixer M2, hydrogen is added by a recycling stream to ensure a reducing environment

https://doi.org/10.52202/077185-0043

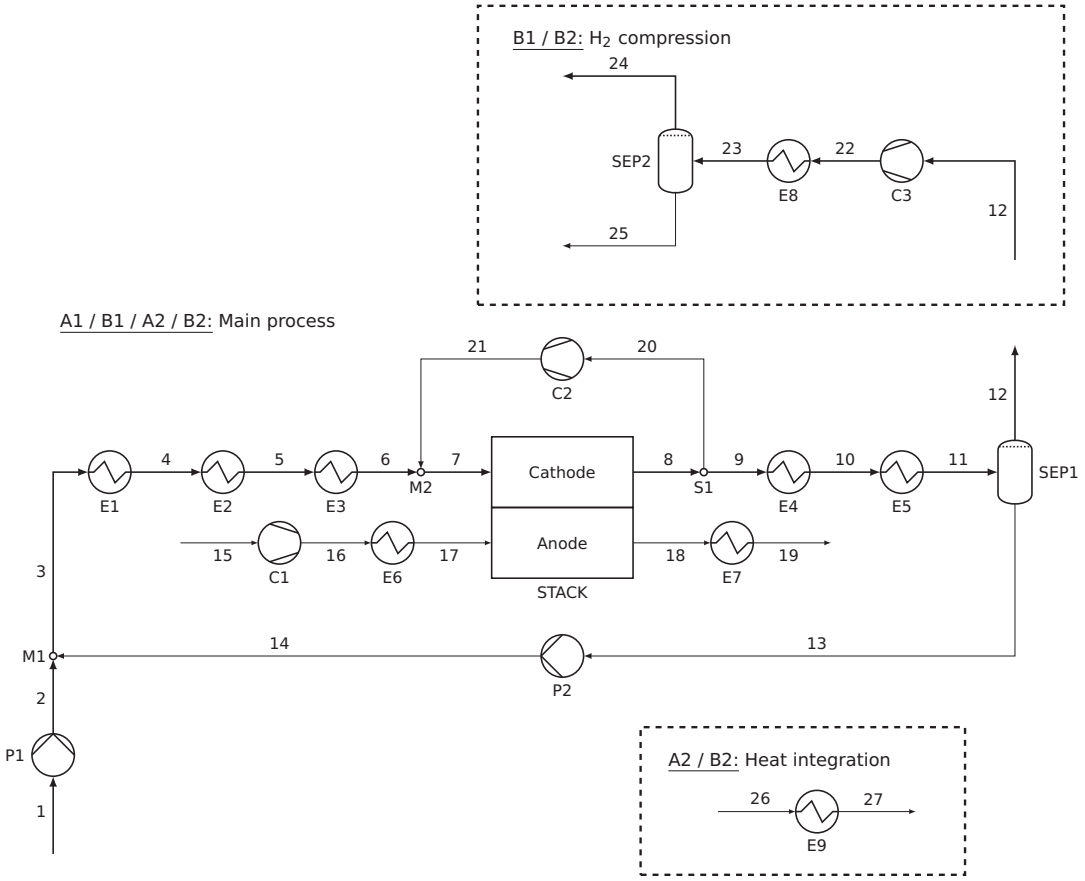

Figure 1: Combined flowsheet of the four SOEL design options analyzed in this study. The framed subsystems are added to the respective designs.

at the cathode inlet. On the anode side, sweep air is first compressed (C1) and then brought to stack temperature in heat exchanger E6.

The stack is modeled according to the approach in Cinti et al., 2016. Thermoneutral operation is assumed in all cases. The electricity supply of the stack requires an AC/DC conversion through a rectifier (RECT) which is not shown in the flowsheet. A portion of the outlet hydrogen-vapor mixture is separated in splitter S1 as a recycle stream and the pressure losses occurring in the stack are compensated for by blower C2. The main part of the product stream is cooled down to the dew point in cooler E4, then the remaining steam is condensed in condenser E4 and the liquid water is removed in separator SEP1 and recycled. The oxygen-enriched sweep air is cooled (E7) and released to the environment.

For the near-atmospheric designs B1 and B2, the pressure of the hydrogen-rich stream must then be increased by compressor C3 in order to provide the inlet pressure for the ammonia synthesis loop. Due to the associated increase in temperature, cooling and water condensation (E8) and separation (SEP2) take place again afterwards. As a result, the hydrogen provided is available at the same temperature and pressure level and has a similar purity in all the design variants under consideration.

In case of designs A2 and B2, the heat of reaction released during ammonia synthesis is removed via the Dowtherm-A cooling circuit shown in Penkuhn, 2023 which is used there similarly to provide high-pressure steam. In the present work, heat exchanger E9 is used to integrate the thermal energy of 14.9 MW into the electrolysis process by cooling down the Dowtherm-A stream (26) from 375–300 K. In this way, the required electrically supplied heat demand is reduced.

https://doi.org/10.52202/077185-0043

Table 1: Model parameters and assumptions used in this study.

Component/Parameter		Design A1/A2	Design B1/B2	Component/Parameter		Design A1/A2	Design B1/B2
Ambient				Separators			
Temperature	°C	15	15	Pressure drop	bar	0.5	0.03
Pressure	bar	1.01325	1.01325	Isentropic efficiencies			
Stack				Compressor C1	%	88	88
Temperature	°C	800	800	Blower C2	%	70	70
Pressure	bar	25	1.5	Compressor C3	%	-	80
H_2 inlet molar fraction	%	10	10	Pump P1 & P2	%	70	70
Steam conversion	%	90	90	Mechanical efficiencies			
Air ratio	-	0.5	0.5	Compressor C1	%	98	98
Pressure drop	bar	0.5	0.03	Blower C2	%	95	95
Rectifier efficiency	%	98	98	Compressor C3	%	-	98
Heat Exchangers				Pump P1 & P2	%	95	95
Min. temp. difference	K	20	20	H_2 output requirement			
Condenser end temp.	°C	40	40	Mass flow	$kg\,s^{-1}$	1	1
Pressure drop	bar	0.5	0.03/0.5	Pressure	bar	23	23

2.2 Model parameters

The main model parameters on which the simulation is based are shown in Table 1. Two important design parameters for the design of SOEL systems are the air ratio AR and the steam conversion SC. The air ratio is defined as the inlet in relation to the produced oxygen mole flow rate.

$$AR = \frac{\dot{n}_{O_2,\text{in}}}{\dot{n}_{O_2,\text{prod}}} \tag{1}$$

Sweep air is often used instead of producing pure oxygen because handling the latter at such high temperatures places higher safety requirements (Buttler and Spliethoff, 2018). Min et al., 2022 collected values for the air ratio of 0.5–1.53 for various experimentally verified SOEL systems. As the compressor power consumption increases with the volume flow and therefore with increasing air ratio, the minimum value of 0.5 is chosen here. Some theoretical studies have also investigated lower values on a system scale, e.g. Wang et al., 2019.

According to Min et al., 2022, the applied steam conversion usually varies between 60–90 %. In the present study, a value of 90 % is selected which can also be achieved by commercially available stacks (Posdziech et al., 2019). The pressure drops are based on AlZahrani and Dincer, 2017 where $\approx 2\,\%$ are assumed as pressure drops in the electrolysis stack and heat exchangers. Furthermore, apart from mechanical/electrical efficiencies, all components are assumed to be adiabatic. The Peng-Robinson equation of state with Boston-Mathias modifications is applied for calculating the thermodynamic properties.

3 METHODOLOGY

Pinch analysis and exergy analysis are two well-established methods for the design and evaluation of material and energy conversion plants. Pinch analysis offers a systematic approach in order to make statements about the possibilities of internal heat recovery and the requirement for external heating and cooling for a given process design and its parameters (Bejan et al., 1996). Exergy analysis, on the other hand, enables a comprehensive understanding of the true thermodynamic inefficiencies occurring in a process and its components in a way that no other method is capable of (Tsatsaronis, 1999). This provides

https://doi.org/10.52202/077185-0043

the opportunity to identify improvement options both in terms of the choice of process parameters at the component level as well as regarding the selection and combination of components at the system level.

3.1 Pinch analysis

The aim of the pinch analysis is to determine the pinch point and the minimum heating and cooling requirements for a set of cold and hot streams with a specified minimum temperature difference $\Delta T_{\min}$ and with knowledge of all mass flows, specific heat capacities and temperatures of the streams. In addition, the minimum temperature of the external heat supply and the maximum temperature of the external cooling source can be determined. A detailed description on the implementation of a pinch analysis can be found in Bejan et al., 1996.

In this study, a minimum temperature difference of $\Delta T_{\min}$=20 K is selected. It should further be noted that pressure drops are neglected in the pinch analysis and the specific heat capacities of the material flows are assumed to be constant - in contrast to the simulation of the SOEL systems in Aspen Plus® described in the previous section. This would result in differences to the results obtained from the pinch analysis when implementing a HEN with maximum energy recovery (MER). However, it is assumed here that these deviations are sufficiently small to show general differences between the process designs.

3.2 Exergy analysis

Exergy represents the maximum theoretical useful work that is obtained when a system or material stream is brought into complete thermodynamic equilibrium with its environment while interacting only with this environment (Tsatsaronis, 2007). As part of an exergy analysis, the total exergy can be split up further with varying degrees of detail. In the following, the total exergy $\dot{E}_i$ of a material stream i consisting of chemical species j is expressed as the sum of the physical and chemical exergy (Tsatsaronis, 2007):

$$\dot{E}_i = \dot{n}_i \left(\overline{e}_i^{\mathrm{PH}} + \overline{e}_i^{\mathrm{CH}}\right) \tag{2}$$

$$\overline{e}_i^{\mathrm{PH}} = \overline{h}_i - \overline{h}_{0,i} + T_0 \left(\overline{s}_i - \overline{s}_{0,i}\right) \tag{3}$$

$$\overline{e}_i^{\mathrm{CH}} = \sum_j x_{j,i}\, \overline{e}_j^{\mathrm{CH}} + \overline{R}\, T_0 \sum_j x_{j,i} \ln x_{j,i} \tag{4}$$

with the molar physical exergy $\overline{e}_i^{\mathrm{PH}}$ and the molar chemical exergy $\overline{e}_i^{\mathrm{CH}}$. The reference environment model by Szargut et al., 1988 is used in this study for the calculation of the standard chemical exergies.

The exergetic efficiency of an overall process is defined as the ratio of the exergetic product to the exergetic fuel while the former can also be expressed as the difference between fuel, exergy loss and exergy destruction (Bejan et al., 1996).

$$\varepsilon_{\mathrm{tot}} = \frac{\dot{E}_{\mathrm{P}}}{\dot{E}_{\mathrm{F}}} = 1 - \frac{\dot{E}_{\mathrm{L}} + \dot{E}_{\mathrm{D}}}{\dot{E}_{\mathrm{F}}} \tag{5}$$

For the SOEL systems shown in Figure 1, the exergetic fuel is defined as the sum of the inlet water, the total electrical power consumed by the stack, compressors and pumps $\dot{W}_{\mathrm{el,tot}}$ as well as the electrical power which is consumed by the electrical heaters $\dot{Q}_{\mathrm{el,Heat}}$. With the integration of the reaction heat of the ammonia synthesis, the decrease in the physical exergy of the heat transfer fluid must also be taken into account. The exergetic product is the sum of the chemical exergy flow of the hydrogen of stream 12 respective 24 and the corresponding physical exergy flow. The water portion of this stream and the pressurized, enriched sweep air stream 19 leaving the system are considered as exergy loss.

$$\mathrm{A1/B1:} \quad \dot{E}_{\mathrm{F}} = \dot{E}_1 + \dot{W}_{\mathrm{el,tot}} + \dot{Q}_{\mathrm{el,Heat}} \tag{6}$$

$$\mathrm{A2/B2:} \quad \dot{E}_{\mathrm{F}} = \dot{E}_1 + \dot{W}_{\mathrm{el,tot}} + \dot{Q}_{\mathrm{el,Heat}} + \dot{E}_{26}^{\mathrm{PH}} - \dot{E}_{27}^{\mathrm{PH}} \tag{7}$$

$$\dot{E}_{\mathrm{P}} = \dot{n}_{\mathrm{H_2},12/24}\, \overline{e}_{\mathrm{H_2}}^{\mathrm{CH}} + \dot{E}_{12/24}^{\mathrm{PH}} \tag{8}$$

$$E_{\mathrm{L}} = \dot{n}_{\mathrm{H_2O},12/24}\, \overline{e}_{\mathrm{H_2O}}^{\mathrm{CH}} + \dot{E}_{19} - \dot{E}_{15} \tag{9}$$

https://doi.org/10.52202/077185-0043

With this definition, all heat that may be dissipated to cooling media is considered as exergy destruction; thus, neither the cooling medium has to be modeled nor does the temperature during heat transfer need to be determined. The total electrical power consumed $\dot{W}_{\mathrm{el,tot}}$ consists of the electrical power of the stack and the sum of compressors and pumps.

$$\dot{W}_{\mathrm{el,tot}} = \dot{W}_{\mathrm{el,STACK,AC}} + \sum \dot{W}_{\mathrm{el,C}} + \sum \dot{W}_{\mathrm{el,P}} \tag{10}$$

On the component level, the exergetic product of the electrolysis stack is defined as the increase in chemical exergy between the inlet and outlet of both streams as well as the increase in physical exergy on the anode side due to diffusion of oxygen ions through the electrolyte, which overcompensates for the pressure drop. The exergetic fuel is expressed as the sum of the electrical power consumed and the decrease in physical exergy on the cathode side due to the pressure drop.

$$\varepsilon_{\mathrm{STACK}} = \frac{\dot{E}_8^{\mathrm{CH}} - \dot{E}_7^{\mathrm{CH}} + \dot{E}_{18}^{\mathrm{CH}} - \dot{E}_{17}^{\mathrm{CH}} + \dot{E}_{18}^{\mathrm{PH}} - \dot{E}_{17}^{\mathrm{PH}}}{\dot{W}_{\mathrm{el,STACK,DC}} + \dot{E}_7^{\mathrm{PH}} - \dot{E}_8^{\mathrm{PH}}} \tag{11}$$

The exergetic product of pumps and compressors is the increase in physical exergy of the transported fluid while the exergetic fuel is the consumed electrical power.

$$\varepsilon_{\mathrm{C/P}} = \frac{\dot{E}_{\mathrm{out}}^{\mathrm{PH}} - \dot{E}_{\mathrm{in}}^{\mathrm{PH}}}{\dot{W}_{\mathrm{el,C/P}}} \tag{12}$$

The purpose of the separators is to increase the chemical exergy of the hydrogen portion of the respective stream. Therefore, this is defined as the exergetic product. The separation takes place at the expense of the chemical exergy of the water portion of the original stream which therefore represents the exergetic fuel as well as the decrease in physical exergy due to the pressure drop.

$$\varepsilon_{\mathrm{SEP1/2}} = \frac{\dot{n}_{12/24}\,(\overline{e}_{12/24}^{\mathrm{CH}} - \overline{e}_{11/23}^{\mathrm{CH}})}{\dot{n}_{13/25}\,(\overline{e}_{11/23}^{\mathrm{CH}} - \overline{e}_{13/25}^{\mathrm{CH}}) + E_{11/23}^{\mathrm{PH}} - \dot{E}_{12/24}^{\mathrm{PH}} - \dot{E}_{13/25}^{\mathrm{PH}}} \tag{13}$$

The mixing units used in the systems investigated are regarded as dissipative components, as their application here is motivated by technical and not thermodynamic reasons (Lazzaretto and Tsatsaronis, 2006). Furthermore, no exergetic efficiencies are specified for the heat exchangers, as these depend on the specific interconnection in the HEN. This will be integrated at a later stage. However, if the remaining components are known, the total cumulative exergy destruction in the heat exchangers $\dot{E}_{\mathrm{D,E,tot}}$ can be calculated by subtraction from the overall process exergy destruction $\dot{E}_{\mathrm{D,tot}}$.

$$\dot{E}_{\mathrm{D,E,tot}} = \dot{E}_{\mathrm{D,tot}} - \sum_{\substack{k \\ k \neq \mathrm{E}}} \dot{E}_{\mathrm{D,k}} \tag{14}$$

This value includes the exergy dissipated to cooling media mentioned above.

Besides these exergy-based considerations, energetic efficiencies of the overall process are calculated based on both the molar lower heating value $\overline{\mathrm{LHV}}$ and the molar higher heating value $\overline{\mathrm{HHV}}$.

$$\mathrm{A1/B1}: \quad \eta_{\mathrm{LHV}} = \frac{\dot{n} \cdot \overline{\mathrm{LHV}}}{\dot{W}_{\mathrm{el,tot}} + \dot{Q}_{\mathrm{el,Heat}}} \tag{15}$$

$$\mathrm{A2/B2}: \quad \eta_{\mathrm{LHV}} = \frac{\dot{n} \cdot \overline{\mathrm{LHV}}}{\dot{W}_{\mathrm{el,tot}} + \dot{Q}_{\mathrm{el,Heat}} + \dot{Q}_{\mathrm{E9}}} \tag{16}$$

$$\mathrm{A1/B1}: \quad \eta_{\mathrm{HHV}} = \frac{\dot{n} \cdot \overline{\mathrm{HHV}}}{\dot{W}_{\mathrm{el,tot}} + \dot{Q}_{\mathrm{el,Heat}}} \tag{17}$$

$$\mathrm{A2/B2}: \quad \eta_{\mathrm{HHV}} = \frac{\dot{n} \cdot \overline{\mathrm{HHV}}}{\dot{W}_{\mathrm{el,tot}} + \dot{Q}_{\mathrm{el,Heat}} + \dot{Q}_{\mathrm{E9}}} \tag{18}$$

Except for the terms $\dot{W}_{\mathrm{el,tot}}$ and $\dot{Q}_{\mathrm{el,Heat}}$, these expressions differ from the definitions in Equations (5) to (8) by replacing the exergetic by energetic quantities and the absence of the inlet water exergy rate.

https://doi.org/10.52202/077185-0043

4 RESULTS AND DISCUSSION

The stream data and the component simulation results of the pressurized designs A1/A2 and the near-atmospheric designs B1/B2 are listed in Table 2 and Table 3.

The lower pressure level in B1/B2 results in a significantly lower evaporator inlet temperature than in A1/A2. This shifts the heat demand from the preheater E1 to the evaporator E2 and the superheater E3. Furthermore, the higher compression in A1/A2 results in a significantly higher compressor outlet temperature and power consumption. This reduces the heat rate required in the anode preheater E6 compared to the near-atmospheric design. The latter shows a lower required stack power, as the reaction enthalpy to be applied to water splitting increases with the pressure.

The expectation stated in the literature that a pressurized operation results in a lower overall power consumption for compression cannot be confirmed in the systems under consideration. The reason for this is the high power required by the anode-side sweep air compressor C1, which must provide a similar pressure as applied on the cathode side in order to avoid material problems. In the pressurized designs A1/A2, this power exceeds the sum of both compressors C1 and C3 from the near-atmospheric designs B1/B2. In the latter, a lower volume flow must be compressed to a slightly lower pressure in C3 than in C1 under pressurized operation. The volume flow to be compressed in C1 is determined by the air ratio AR, meaning that the choice of the latter directly influences the power consumption of C1.

Table 2: Stream data simulation results for the different SOEL designs.

	Design A1/A2					Design B1/B2				
No.	$\dot{n}$ mol s^{-1}	T °C	p bar	$\overline{e}^{PH}$ kJ kmol^{-1}	$\overline{e}^{CH}$ kJ kmol^{-1}	$\dot{n}$ mol s^{-1}	T °C	p bar	$\overline{e}^{PH}$ kJ kmol^{-1}	$\overline{e}^{CH}$ kJ kmol^{-1}
1	497.57	15.00	1.01	0.0	900.0	520.13	15.00	1.01	0.0	900.0
2	497.57	15.40	26.50	54.2	900.0	520.13	15.01	1.59	1.2	900.0
3	545.11	17.55	26.50	57.1	900.2	545.13	16.14	1.59	2.6	900.0
4	545.11	225.50	26.00	4627.2	900.2	545.13	113.57	1.56	1137.2	900.0
5	545.11	224.52	25.50	18981.6	900.2	545.13	113.11	1.53	11639.9	900.0
6	545.11	799.74	25.00	33255.4	900.2	545.13	799.27	1.50	26707.1	900.0
7	612.41	800.00	25.00	31154.4	24416.7	612.44	800.00	1.50	24581.2	24416.5
8	612.41	800.00	24.50	20251.1	214880.9	612.44	800.00	1.47	13487.6	214880.9
9	545.11	800.00	24.50	20251.1	214880.9	545.13	800.00	1.47	13487.6	214880.9
10	545.11	121.66	24.00	8278.6	214880.9	545.13	53.12	1.44	1141.1	214880.9
11	545.11	40.00	23.50	6946.8	214880.9	545.13	40.00	1.41	845.7	214880.9
12	497.57	39.94	23.00	7530.4	235355.1	520.13	39.70	1.38	830.6	225164.0
13	47.53	39.94	23.00	134.8	902.3	25.00	39.70	1.38	87.6	900.1
14	47.53	40.00	26.50	142.5	902.3	25.00	39.70	1.59	88.1	900.1
15	598.29	15.00	1.01	0.0	110.9	598.29	15.00	1.01	0.0	110.9
16	598.29	490.29	25.50	13696.3	110.9	598.29	56.05	1.53	1069.6	110.9
17	598.29	800.00	25.00	20571.2	110.9	598.29	800.00	1.50	13781.0	110.9
18	846.32	800.00	24.50	20709.8	463.0	846.33	800.00	1.47	13923.8	463.1
19	846.32	40.00	24.00	7563.8	463.0	846.33	40.00	1.44	876.2	463.1
20	67.30	800.00	24.50	20251.1	214880.9	67.31	800.00	1.47	13487.6	214880.9
21	67.30	808.19	25.00	20489.6	214880.9	67.31	808.18	1.50	13725.2	214880.9
22	-	-	-	-	-	520.13	522.5	24.00	14042.5	225164.0
23	-	-	-	-	-	520.13	40.00	23.50	7274.1	225164.0
24	-	-	-	-	-	497.59	39.93	23.00	7530.4	235355.4
25	-	-	-	-	-	22.54	39.93	23.00	134.7	902.3
26	492.86	375.00	9.00	44415.9	-	492.86	375.00	9.00	44415.9	-
27	492.86	299.87	8.00	28429.3	-	492.86	299.87	8.00	28429.3	-

https://doi.org/10.52202/077185-0043

Table 3: Component simulation results for the different SOEL designs.

		Design A1/A2	Design B1/B2			Design A1/A2	Design B1/B2
$\dot{W}_{el}$ (kW):	STACK (AC)	125852.67	125700.63	$\dot{Q}$ (kW):	E1	9665.36	4339.11
	STACK (DC)	123335.62	123186.62		E2	18586.98	22540.35
	P1	40.21	0.95		E3	12646.56	14242.52
	P2	0.54	0.02		E4	-11263.34	-12337.62
	C1	8773.96	730.27		E5	-3433.69	-1339.23
	C2	18.36	18.3		E6	6058.07	13911.82
	C3	-	7598.46		E7	-20685.83	-20353.45
	Total	134685.74	134048.62		E8	-	-8458.11
					E9	14911.76	14911.76

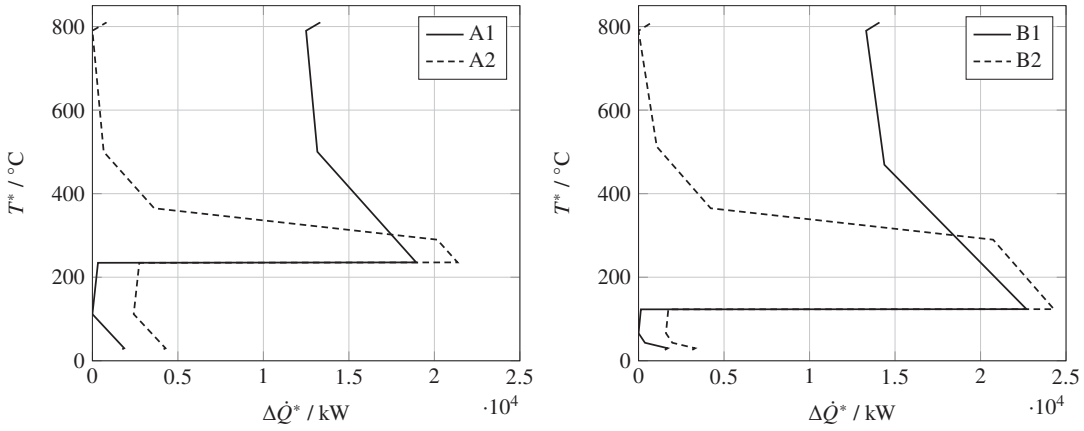

Figure 2: Grand composite curves of the designs before (A1/B1) and after (A2/B2) heat integration.

4.1 Pinch analysis

The results of the pinch analysis are listed in Table 4 and the resulting grand composite curves are displayed in Fig. 2. In the standalone variant, design A1 has a higher pinch point than design B1 due to the higher evaporation temperature. The heat integration from the ammonia synthesis in designs A2 and B2 shifts the pinch point up to the stack temperature (hot side), as the hot utility required in A1 and B1 can be almost completely covered by the integrated reaction heat. Only for heating the steam and the sweep air above 780 °C, hot utility in the form of electrical energy $\dot{Q}_{el,Heat}$ must still be used due to the minimum temperature difference in the heat exchangers. Since the integrated reaction heat $\dot{Q}_{E9}$ provided by heat exchanger E9 exceeds the heating demand in the respective temperature ranges, the cold utility increases in both designs. A part of the heat to be removed is available at a high-temperature level of 800 °C which makes the coupling of subsequent thermal power processes conceivable.

4.2 Exergy analysis

Table 5 shows the exergy analysis results at the component and overall process level. Without heat integration of the ammonia synthesis, the pressurized design A1 has a slightly higher exergetic efficiency than the near-atmospheric design B1.

At the component level, the pressurized designs show a notably lower exergy destruction in the stack and also, cumulative, in the heat exchangers. While the former is due to the fact that water splitting is a

https://doi.org/10.52202/077185-0043

Table 4: Pinch analysis results for the different SOEL designs.

		Design A1	Design A2	Design B1	Design B2
Pinch temperatures (cold/hot)	°C	101.7/121.7	780.0/800.0	56.1/76.1	780.0/800.0
Heating demand	kW	46956.97	46956.97	55033.8	55033.8
Cooling demand	kW	35382.86	50294.63	42488.41	57400.17
Hot utility target	kW	13321.02	825.26	14083.16	774.07
Cold utility target	kW	1746.92	4162.91	1537.77	3140.44
Heat recovery target	kW	33635.95	46131.71	40950.64	54259.73

Table 5: Exergy and energy analysis results for the different SOEL designs.

			Design A1	Design A2	Design B1	Design B2
RECT	$\dot{E}_{\mathrm{D},k}$	kW	2517.05	2517.05	2514.01	2514.01
	ε_k	%	98.00	98.00	98.00	98.00
STACK	$\dot{E}_{\mathrm{D},k}$	kW	7825.86	7825.86	9468.83	9468.83
	ε_k	%	93.98	93.98	92.72	92.72
P1	$\dot{E}_{\mathrm{D},k}$	kW	13.24	13.24	0.31	0.31
	ε_k	%	67.07	67.07	67.06	67.06
P2	$\dot{E}_{\mathrm{D},k}$	kW	0.17	0.17	0.01	0.01
	ε_k	%	68.77	68.77	68.75	68.75
C1	$\dot{E}_{\mathrm{D},k}$	kW	579.52	579.52	90.34	90.34
	ε_k	%	93.39	93.39	87.63	87.63
C2	$\dot{E}_{\mathrm{D},k}$	kW	2.32	2.32	2.31	2.31
	ε_k	%	87.39	87.39	87.4	87.4
C3	$\dot{E}_{\mathrm{D},k}$	kW	-	-	726.50	726.50
	ε_k	%	-	-	90.44	90.44
SEP1	$\dot{E}_{\mathrm{D},k}$	kW	17.06	17.06	26.80	26.80
	ε_k	%	99.83	99.83	99.50	99.50
SEP2	$\dot{E}_{\mathrm{D},k}$	kW	-	-	17.04	17.04
	ε_k	%	-	-	99.67	99.67
M1	$\dot{E}_{\mathrm{D},k}$	kW	2.60	2.60	1.42	1.42
	ε_k	%	-	-	-	-
M2	$\dot{E}_{\mathrm{D},k}$	kW	427.47	427.47	428.2	428.2
	ε_k	%	-	-	-	-
E, tot (with MER)	$\dot{E}_{\mathrm{D},k}$	kW	9464.5	4847.87	13373.68	7943.72
	ε_k	%	-	-	-	-
Total (with MER)	$\dot{E}_{\mathrm{F,tot}}$	kW	148454.58	143837.94	148599.90	143169.94
	$\dot{E}_{\mathrm{P,tot}}$	kW	120863.38	120863.38	120868.80	120868.80
	$\dot{E}_{\mathrm{L,tot}}$	kW	6741.41	6741.41	1081.65	1081.65
	$\dot{E}_{\mathrm{D,tot}}$	kW	20849.79	16233.15	26649.45	21219.49
	$\varepsilon_{\mathrm{tot}}$	%	81.41	84.03	81.34	84.42
	$\dot{Q}_{\mathrm{el,Heat}}$	kW	13321.02	825.26	14083.16	774.07
	$\dot{W}_{\mathrm{el,tot}}$	kW	134685.74	134685.74	134048.62	134048.62
	η_{LHV}	%	81.04	79.74	80.97	80.11
	η_{HHV}	%	95.79	94.25	95.71	94.69

https://doi.org/10.52202/077185-0043

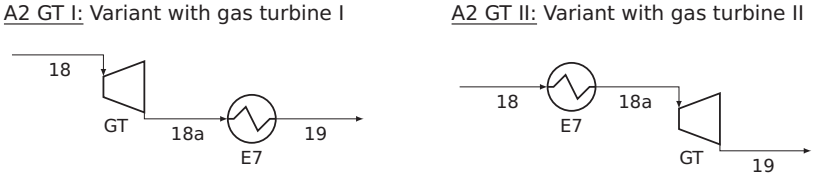

Figure 3: Extended process variants of design A2 with a gas turbine for sweep gas utilization.

volume-increasing reaction in which an increase in pressure is thermodynamically favorable, the latter is due to the higher temperature level during evaporation and the lower hot utility requirement provided by electrical heat (see Table 4). Furthermore, the sum of the exergy destructions of compressors C1 and C3 in designs B1/B2 is higher than the exergy destruction of compressor C1 in the pressurized designs A1/A2. At the same time, compressor C1 in the pressurized designs and C3 in the near-atmospheric designs show high exergetic efficiencies since, in both cases, significant temperature increases occur during compression and exergy destruction due to friction decreases with temperature. In addition, the pressurized designs have significantly higher exergy losses due to the higher sweep air outlet pressure. Therefore, it is concluded that the air ratio would significantly affect the results, as it influences both the compressor power consumption and exergy destruction of C1 and the exergy loss of the overall system.

The heat integration of ammonia synthesis and the associated lower electrically supplied heat demand significantly reduces the cumulative exergy destruction in the heat exchangers, whereby this is even more the case in the near-atmospheric design than in the pressurized design due to a lower cold utility increase. This further increases the exergetic efficiency by 2.6 and 3.5 percentage points, respectively, which makes the atmospheric design more efficient.

Table 5 also lists the energetic efficiencies η_{LHV} and η_{HHV} of the considered systems. In contrast to the exergetic approach, a decrease in the energetic efficiency occurs with the heat integration of the ammonia synthesis. Although the decrease in the electrically supplied hot utility is also taken into account in Equations (15) to (18), this is energetically overcompensated by the integrated heat from the ammonia synthesis, which leads to an increase in cold utility and, thus, energy loss. However, this does not take into account the fact that the exergy difference ($\dot{E}_{26}^{\mathrm{PH}} - \dot{E}_{27}^{\mathrm{PH}} = 7879.2\,\mathrm{kW}$) provided by the heat transfer fluid is smaller than the corresponding heat flow and that the substituted hot utility is supplied as electrical energy and thus pure exergy. The purely energetic approach is not able to take into account qualitative differences in the heat supplied and, therefore, provides misleading results.

4.3 Additional sweep air utilization

Decreasing the air ratio was mentioned as a measure to avoid the high exergy loss in the pressurized designs associated with the exiting sweep air. Another option would be the utilization of the sweep air outlet stream in a gas turbine. Two variants for this approach are shown in Fig. 3 for the pressurized design A2. In a subsequent study, for both cases, an isentropic efficiency of $\eta_{\mathrm{s,GT}} = 0.9$, a pressure drop of $\Delta p \approx 2\,\%$ in the subsequent heat exchanger E7, and the same system outlet pressure of 1.44 bar (stream 19) as in the near-atmospheric designs are assumed to compare both variants.

The gas turbine in design A2 GT I provides an electric power of 13 435 kW, which would be more than enough to cover the power of 8774 kW required by the sweep air compressor C1 (see Table 3). The exergetic efficiency increases by 1.2 percentage points to 85.21 %. In the design A2 GT II, the gas turbine can provide an electric power of 7472 kW, and an even higher exergetic efficiency of 86.26 % can be reached even though the provided electrical power is lower. This is due to the fact that a considerable part of the enthalpy of the hot sweep air is also required for internal heat recovery, which can be utilized in a more favorable ratio in the A2 GT II design. A more detailed discussion of these cases will be provided elsewhere.

https://doi.org/10.52202/077185-0043

5 CONCLUSIONS

The present study compares a pressurized and a near-atmospheric SOEL system with and without heat integration of a subsequent ammonia synthesis process based on pinch and exergy analyses. The pinch analysis shows that the hot utility provided electrically in the standalone variant can be almost entirely replaced by the reaction heat of the ammonia synthesis through heat integration. A comparison based on the exergy analysis shows that the exergetic efficiency thus increases in both cases, while the energetic efficiency decreases misleadingly.

Furthermore, it is observed that in the standalone variant, the pressurized design shows slight efficiency advantages over the near-atmospheric variant, but this is reversed by heat integration. Due to the high compressor power consumption and high exergy losses in the pressurized design due to the sweep air usage, it is concluded that the air ratio significantly influences the overall efficiency. It is also demonstrated that with sweep air utilization, significant efficiency improvements can be achieved in the pressurized design, resulting in the highest exergetic efficiencies. The latter two findings will be investigated in more detail in the future. In addition, future studies should consider the influence of the operating pressure on the electrochemical resistance and, thus, on the required electrolysis area for a holistic view.

NOMENCLATURE

Abbreviations

C	Compressor	MER	Maximum energy recovery
E	Heat Exchanger	P	Pump
GT	Gas turbine	RECT	Rectifier
HEN	Heat exchanger network	SEP	Separator
M	Mixer	SOEL	Solid-oxide electrolysis

Latin Symbols

AR	Air ratio	–	$\dot{Q}$	Heat rate	kW
$\overline{e}$	Molar exergy	kJ kmol^{-1}	p	Pressure	bar
$\dot{E}$	Exergy rate	kW	$\overline{s}$	Molar entropy	kJ kmol^{-1}
$\overline{h}$	Molar enthalpy	kJ kmol^{-1}	$\dot{W}$	Power	kW
$\overline{\text{HHV}}$	Higher heating value	kJ kmol^{-1}	T	Temperature	°C
$\overline{\text{LHV}}$	Lower heating value	kJ kmol^{-1}	x	Molar fraction	–
$\dot{n}$	Mole flow rate	mol s^{-1}			

Greek Symbols

ε	Exergetic efficiency	%	η	Energetic efficiency	%

Superscripts and Subscripts

el	Electrical	D	Destruction
i	Stream	F	Fuel
j	Species	Heat	Heater
k	Component	L	Loss
tot	Total	P	Product
CH	Chemical	PH	Physical

REFERENCES

AlZahrani, A. A. and I. Dincer (2017). "Thermodynamic and Electrochemical Analyses of a Solid Oxide Electrolyzer for Hydrogen Production". In: *Int. J. Hydrog. Energy* 42.33, pp. 21404–21413. DOI: 10.1016/j.ijhydene.2017.03.186.

Appl, M. (2011). "Ammonia, 2. Production Processes". In: *Ullmann's Encyclopedia of Industrial Chemistry*. 1st ed. John Wiley & Sons, Ltd. DOI: 10.1002/14356007.o02_o11.

https://doi.org/10.52202/077185-0043

Bejan, A., G. Tsatsaronis, and M. J. Moran (1996). *Thermal Design and Optimization*. A Wiley-Interscience Publication. New York: Wiley. ISBN: 978-0-471-58467-4.

Buttler, A. and H. Spliethoff (2018). "Current Status of Water Electrolysis for Energy Storage, Grid Balancing and Sector Coupling via Power-to-Gas and Power-to-Liquids: A Review". In: *Renew. Sustain. Energy Rev.* 82, pp. 2440–2454. DOI: 10.1016/j.rser.2017.09.003.

Cinti, G. et al. (2016). "Integration of Solid Oxide Electrolyzer and Fischer-Tropsch: A Sustainable Pathway for Synthetic Fuel". In: *Appl. Energy* 162, pp. 308–320. DOI: 10.1016/j.apenergy.2015.10.053.

Deutschmann, O. et al. (2011). "Heterogeneous Catalysis and Solid Catalysts, 3. Industrial Applications". In: *Ullmann's Encyclopedia of Industrial Chemistry*. John Wiley & Sons, Ltd. DOI: 10.1002/14356007.o05_o03.

Hansen, J. B., N. Christiansen, and J. U. Nielsen (2011). "Production of Sustainable Fuels by Means of Solid Oxide Electrolysis". In: *ECS Trans.* 35.1, pp. 2941–2948. DOI: 10.1149/1.3570293.

Hauch, A. et al. (2020). "Recent Advances in Solid Oxide Cell Technology for Electrolysis". In: *Science* 370.6513, eaba6118. DOI: 10.1126/science.aba6118.

Henke, M. et al. (2011). "Influence of Pressurisation on SOFC Performance and Durability: A Theoretical Study". In: *Fuel Cells* 11.4, pp. 581–591. DOI: 10.1002/fuce.201000098.

Jensen, S. H. et al. (2016). "Pressurized Operation of a Planar Solid Oxide Cell Stack". In: *Fuel Cells* 16.2, pp. 205–218. DOI: 10.1002/fuce.201500180.

Jensen, S. H. et al. (2010). "Hydrogen and Synthetic Fuel Production Using Pressurized Solid Oxide Electrolysis Cells". In: *Int. J. Hydrog. Energy* 35.18, pp. 9544–9549. DOI: 10.1016/j.ijhydene.2010.06.065.

Lazzaretto, A. and G. Tsatsaronis (2006). "SPECO: A Systematic and General Methodology for Calculating Efficiencies and Costs in Thermal Systems". In: *Energy* 31.8-9, pp. 1257–1289. DOI: 10.1016/j.energy.2005.03.011.

Luyben, W. L. (2012). "Design and Control of a Cooled Ammonia Reactor". In: *Plantwide Control*. Ed. by G. P. Rangaiah and V. Kariwala. 1st ed. Wiley, pp. 273–292. DOI: 10.1002/9781119968962.ch13.

Min, G., S. Choi, and J. Hong (2022). "A Review of Solid Oxide Steam-Electrolysis Cell Systems: Thermodynamics and Thermal Integration". In: *Appl. Energy* 328, p. 120145. DOI: 10.1016/j.apenergy.2022.120145.

Ott, J. et al. (2012). "Methanol". In: *Ullmann's Encyclopedia of Industrial Chemistry*. John Wiley & Sons, Ltd. DOI: 10.1002/14356007.a16_465.pub3.

Penkuhn, M. (2023). "Further Development and Application of Advanced Exergy-Based Methods". PhD thesis. Berlin: Technische Universität Berlin.

Penkuhn, M. and G. Tsatsaronis (2017). "Comparison of Different Ammonia Synthesis Loop Configurations with the Aid of Advanced Exergy Analysis". In: *Energy* 137, pp. 854–864. DOI: 10.1016/j.energy.2017.02.175.

Posdziech, O., K. Schwarze, and J. Brabandt (July 2019). "Efficient Hydrogen Production for Industry and Electricity Storage via High-Temperature Electrolysis". In: *Int. J. Hydrog. Energy* 44.35, pp. 19089–19101. DOI: 10.1016/j.ijhydene.2018.05.169.

Riedel, M., M. P. Heddrich, and K. A. Friedrich (2019). "Analysis of Pressurized Operation of 10 Layer Solid Oxide Electrolysis Stacks". In: *Int. J. Hydrog. Energy* 44.10, pp. 4570–4581. DOI: 10.1016/j.ijhydene.2018.12.168.

Riedel, M., M. P. Heddrich, and K. A. Friedrich (2020). "Experimental Analysis of the Co-Electrolysis Operation under Pressurized Conditions with a 10 Layer SOC Stack". In: *J. Electrochem. Soc.* 167.2, p. 024504. DOI: 10.1149/1945-7111/ab6820.

Rouwenhorst, K. H. R. et al. (2020). "Ammonia, 4. Green Ammonia Production". In: *Ullmann's Encyclopedia of Industrial Chemistry*. 1st ed. John Wiley & Sons, Ltd, pp. 1–20. DOI: 10.1002/14356007.w02_w02.

Samavati, M. et al. (2018). "Integration of Solid Oxide Electrolyser, Entrained Gasification, and Fischer-Tropsch Process for Synthetic Diesel Production: Thermodynamic Analysis". In: *Int. J. Hydrog. Energy* 43.10, pp. 4785–4803. DOI: 10.1016/j.ijhydene.2018.01.138.

Szargut, J., D. R. Morris, and F. R. Steward (1988). *Exergy Analysis of Thermal, Chemical, and Metallurgical Processes*. New York: Hemisphere. ISBN: 978-0-89116-574-3.

The Royal Society (2020). *Ammonia: Zero-Carbon Fertiliser, Fuel and Energy Store*. Tech. rep. ISBN: 978-1-78252-448-9. London: The Royal Society.

Tsatsaronis, G. (1999). "Strengths and Limitations of Exergy Analysis". In: *Thermodynamic Optimization of Complex Energy Systems*. Ed. by A. Bejan and E. Mamut. Dordrecht: Springer Netherlands, pp. 93–100. DOI: 10.1007/978-94-011-4685-2_6.

Tsatsaronis, G. (2007). "Definitions and Nomenclature in Exergy Analysis and Exergoeconomics". In: *Energy* 32.4, pp. 249–253. DOI: 10.1016/j.energy.2006.07.002.

Wang, L. et al. (2019). "Trade-off Designs and Comparative Exergy Evaluation of Solid-Oxide Electrolyzer Based Power-to-Methane Plants". In: *Int. J. Hydrog. Energy* 44.19, pp. 9529–9543. DOI: 10.1016/j.ijhydene.2018.11.151.

https://doi.org/10.52202/077185-0043